FEBS Letters

FEBS PRESS science publishing by scientists

RESEARCH LETTER

Heparin promotes rapid fibrillation of the basic parathyroid hormone at physiological pH

Luca M. Lauth[1], Bruno Voigt[2], Twinkle Bhatia[1], Lisa Machner[3], Jochen Balbach[2] and Maria Ott[2]

1 Department of Biochemistry and Biotechnology, Martin-Luther-University Halle-Wittenberg, Germany
2 Department of Biophysics, Martin-Luther-University Halle-Wittenberg, Germany
3 Department of Molecular Medicine, Martin-Luther-University Halle-Wittenberg, Germany

Correspondence
L. M. Lauth and M. Ott, Department of Biochemistry and Biotechnology, Martin-Luther-University Halle-Wittenberg, Halle, Germany
Tel: +49 (0)345 5 524 946
E-mail: luca.lauth@bct.uni-halle.de (LML); maria.ott@bct.uni-halle.de (MO)

(Received 19 March 2022, revised 14 June 2022, accepted 9 July 2022, available online 9 August 2022)

doi:10.1002/1873-3468.14455

Edited by Barry Halliwell

In acidic secretory granules of mammalian cells, peptide hormones including the parathyroid hormone are presumably stored in the form of functional amyloid fibrils. Mature PTH, however, is considerably positively charged in acidic environments, a condition known to impede unassisted self-aggregation into fibrils. Here, we studied the role of the polyanion heparin on promoting fibril formation of PTH. Employing ITC, CD spectroscopy, NMR, SAXS, and fluorescence-based assays, we could demonstrate that heparin binds PTH with submicromolar affinity and facilitates its conversion into fibrillar seeds, enabling rapid formation of amyloid fibrils under acidic conditions. In the absence of heparin, PTH remained in a soluble monomeric state. We suspect that heparin-like surfaces are required *in vivo* to convert PTH efficiently into fibrillar deposits.

Keywords: acidic pH; amyloid fibrillation; functional amyloids; heparin interaction; intrinsically disordered proteins; parathyroid hormone

The parathyroid hormone (PTH) is a peptide hormone expressed in parathyroid chief cells that binds the PTH-specific G protein-coupled receptors PTH1R and PTH2R to regulate serum calcium ion and phosphate levels [1–4]. Like any peptide hormone, PTH needs to be secreted from the producing cells to enable its access to the target structures *via* the blood stream [5] (Fig. 1A). For that purpose, peptide hormones are generally destined to pass the secretory pathway. Importantly, the organelles that constitute the secretory pathway get continuously acidified as they approach the state of secretion [6]. The resulting pH gradient across the secretory pathway is implicated in regulating events of post-translational modifications and sorting of cargo proteins. Moreover, the decrease in pH is accompanied by the formation of amyloid fibrils, which is the presumed storage form of peptide hormones inside secretory granules [7–9]. Interestingly, many peptide hormones yield an isoelectric point (pI) close to the acidic pH of approx. 5.5 as found in the trans-Golgi network and secretory granules. Consequently, these proteins are less soluble at low pH while displaying an enhanced propensity to aggregate, for example, into amyloid fibrils [8,10–12]. Indeed, many of these peptide hormones spontaneously fibrillate also *in vitro* at pH 5.5 [7].

Mature PTH (C-terminal 84 amino acids, from now on referred to as $PTH_{1\text{-}84}$), however, has a calculated pI value of 8.9 and harbors four histidine residues with a pK_A value of approximately 6.2. As a result, the net charge of $PTH_{1–84}$ increases significantly under acidifying conditions: While the net charge at pH 7.4 is

Abbreviations
b, length of a Kuhn segment; CD, circular dichroism; GAG, glycosaminoglycan; ITC, isothermal titration calorimetry; κ, rate of secondary nucleation and growth; *L*, contour length; PTH, parathyroid hormone; R_c, cross-sectional radius; R_g, radius of gyration; SAXS, small-angle X-ray scattering; TEM, transmission electron microscopy; ThT, Thioflavin T; WAXS, wide-angle X-ray scattering; λ, rate of primary nucleation and growth.

FEBS Letters **596** (2022) 2928–2939 © 2022 The Authors. *FEBS Letters* published by John Wiley & Sons Ltd on behalf of Federation of European Biochemical Societies.

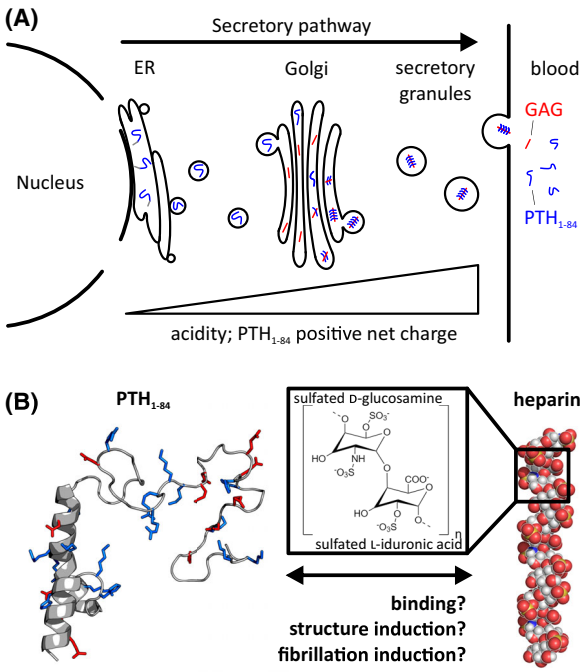

Fig. 1. Research hypothesis based on cellular transport of basic $PTH_{1–84}$ and fibrillation in acidic environments. (A) Illustration of the PTH (blue) passing through the secretory pathway. The pH gradient across the secretory pathway leads to a continuous increase in positive net charge of $PTH_{1–84}$. $PTH_{1–84}$ fibrils are found in acidic secretory granules [9]. GAGs (red) are abundant in the secretory pathway [17,18]. We hypothesize that GAGs interact with $PTH_{1–84}$ and induce its fibrillation. (B) Cartoon representation of $PTH_{1–84}$ based on the PDB entry 1ZWA and a C-terminal disordered region. Charged residues are highlighted in blue (positive) and red (negative). The linear polyanionic heparin consists of repeating sulfated D-glucosamines and L-iduronic acid monosaccharides (black box).

approximately +1.4, it is raised to +5.9 at pH 5.5 [13]. Since $PTH_{1–84}$ is a protein with high structural disorder (Fig. 1B) [14], an increased repulsion between like-charged residues should lead to more extended conformations and enhanced mutual repulsion. Hence, the inherent predisposition for amyloid-prone conformations and the formation of initial amyloid seeds should be affected [15]. Indeed, *in vitro* screening of different buffer conditions revealed that amyloid fibrils form preferably at basic conditions, close to the pI of PTH_{1-84} [14]. This finding contrasts *in vivo* observations of amyloid fibril generation in acidic secretory granules of parathyroid chief cells [9]. Hence, under physiological conditions, fibril formation of $PTH_{1–84}$ requires additional factors to occur. In this study, we tested the hypothesis of a polyanion-assisted fibrillation of $PTH_{1–84}$ by the use of heparin (Fig. 1B), an important and widely used member of the glycosaminoglycan (GAG) family [16]. GAGs are linear polyanionic polysaccharides that are abundant in the secretory pathway [17,18] and known components of amyloid deposits [19]. Notably, the seminal work of Maji and coworkers in 2009 identified GAGs to be essential for *in vivo* fibrillation of numerous peptides and protein hormones found in secretory granules [7]. To our best knowledge, this aspect has not yet been investigated for the parathyroid system with its hormone $PTH_{1–84}$.

With the help of *in vitro* experiments, we could demonstrate that heparin does not only efficiently bind $PTH_{1–84}$, but also increases its ordered secondary structure content and induces rapid fibrillation even at low physiological pH. Moreover, fibrils formed in the presence of heparin were still capable to release monomeric peptides, a typical characteristic of functional amyloid fibrils. In the absence of heparin, $PTH_{1–84}$ was not able to form fibrils.

Material and methods

Material

$PTH_{1–84}$ was synthesized by the Core Unit Peptide Technologies of the University Leipzig using microwave-assisted solid-phase peptide synthesis (CEM GmbH, Kamp-Lintfurt, Germany) based on Fmoc-strategy. For long peptides as $PTH_{1–84}$, the incorporation of selected pseudoprolines leads to products usable for the challenging purification steps after the cleavage from the resin. The successful synthesis of $PTH_{1–84}$ was verified by mass spectrometry. Unfractionated porcine intestinal heparin with an average molecular weight of 20 kDa was sourced from Carl Roth (Carl Roth GmbH, Karlsruhe, Germany). The heparin sulfate analog fondaparinux (pentasaccharide) was sourced from Merck (Merk KGaA, Darmstadt, Germany). Other chemicals were reagent grade and sourced from Sigma-Aldrich (Sigma-Aldrich Chemie GmbH, Schnelldorf, Germany) if not stated otherwise.

Methods

Sample preparation

Lyophilized $PTH_{1–84}$ was dissolved in citrate buffer (20 mM, pH 5.5) or sodium phosphate buffer (50 mM, pH 7.4) and its concentration adjusted *via* UV absorbance at 280 nm ($\varepsilon = 5500\ M^{-1}{\cdot}cm^{-1}$). Heparin or fondaparinux were weighed in and dissolved in the same buffer. Desired heparin concentrations were prepared according to its average mass of 20 kDa.

Circular dichroism spectroscopy

UV circular dichroism (CD) measurements were carried out on a Jasco J-810 spectrophotometer (Jasco Deutschland

GmbH, Pfungstadt, Germany) using a 0.01 cm pathlength quartz cuvette (Hellma GmbH & Co. KG, Müllheim, Germany). The $PTH_{1–84}$ concentration was adjusted to 0.1 mM in citrate buffer (20 mM, pH 5.5) or sodium phosphate buffer (50 mM, pH 7.4). Heparin-containing samples were set to a final molar ratio of 1 : 10 (heparin : PTH_{1-84}) and incubated for 1 h at 20 °C. As the amplitude of the CD signal of heparin was much smaller compared with $PTH_{1–84}$, we corrected the CD spectra of the solution containing $PTH_{1–84}$ and heparin for eventual heparin contributions by adding equal heparin concentrations in the reference buffer. The exposure time was set to 50 nm·min^{-1}, and spectra were obtained from averaging 64 subsequent measurements at 20 °C after subtracting the reference buffer spectrum.

NMR spectroscopy

2D 1H-15 N HSQC spectra of 100 μM 15 N labeled $PTH_{1–84}$ were recorded on a Bruker Ascend 500 MHz spectrometer at pH 5.5 and 25 °C in the absence and presence of 100 μM fondaparinux. Chemical shift assignments were performed by standard triple resonance experiments based on the published values [20].

Isothermal titration calorimetry

Calorimetric measurements were performed using a MicroCal iTC200 (Malvern Panalytical Ltd, Malvern, UK) calorimeter at 25 °C and 750 r.p.m stirring. Titrations of a 125 μM heparin solution into a 150 μM $PTH_{1–84}$ solution, both citrate buffer (20 mM, pH 5.5), were analyzed. The titration regime included an initial 0.5 μL injection and subsequent 39 × 1 μL injections with a time interval of 300 s. The reference cell contained citrate buffer (20 mM, pH 5.5). Thermograms were integrated using NITPIC software (version 1.3.0) [21]. Data fitting was performed using CHASM software with the built-in one-site model and optional use of multi-site models [22].

Wide-angle and small-angle X-ray scattering

All X-ray scattering experiments were performed in vtransmission mode using a SAXSLAB laboratory setup (Retro-F) equipped with an AXO microfocus X-ray source. The AXO multilayer X-ray optic (AXO Dresden GmbH, Dresden, Germany) was used as a monochromator for Cu-K_α radiation ($\lambda = 0154$ nm). A two-dimensional detector (PILATUS3 R 300 K; DECTRIS, Baden, Switzerland) was used to record the 2D scattering patterns. For wide-angle X-ray scattering (WAXS) experiments, fibrils were formed in citrate buffer (20 mM, pH 5.5) in the presence of heparin (1 : 10 molar ratio). The fibril suspension was ultracentrifugated (200 000 x g, 10 min) and the thus obtained pellet transferred into a ring-shaped aluminum holder (2 mm thick and with a central hole of 1.5 mm diameter) and left to dry overnight. The scattering measurements were performed at room temperature in vacuum.

Small-angle X-ray scattering (SAXS) experiments were conducted using refillable capillaries with an outer diameter of 1 mm (BioSAS JSP stage, SAXSLAB/Xenocs SAS, Grenoble, France). The intensities were angular-averaged and plotted versus the scattering angle q. The measurements were performed in citrate buffer (20 mM, pH 5.5), at room temperature and corrected for background, transmission and sample geometry. The measurement times of pure heparin and $PTH_{1–84}$ solutions were 10 h. For the time-dependent series of the mixed solution, 12 consecutive measurements of 2 h each were taken. Due to the lower scattering contrast of heparin and, consequently, the need to measure at higher concentrations, we performed experiments at two concentrations (100 μM and 1 mM) with subsequent extrapolation to zero concentration [23]. The data analysis for all measurements included at first the determination of the radius of gyration, R_g, using the Guinier approximation with $\ln(I(q)) \approx R_g^2/3 \cdot q^2$ for the low q-range, $qR_g < 1.3$. Secondly, the intermediate q-range was fitted to access the shapes of the scatterers using suitable form factor descriptions, $P(q)$. For the scattering of $PTH_{1–84}$, a linear polymer model (Debye function) was used [24]:

$$P(q) = \phi(\Delta\rho)^2 2V_c\left(e^{(qR_g)^2} + \left(qR_g\right)^2 - 1\right)/\left(qR_g\right)^4, \quad (1)$$

where V_c is the chain's volume of occupation, $\Delta\rho$ the scattering contrast, and ϕ the volume fraction.

For solutions of heparin and heparin with $PTH_{1–84}$, a description of a semiflexible chain, as introduced by Pedersen and Schurtenberger [25,26], gave the best fitting result. The main fitting parameters are the so-called Kuhn length, b, reflecting the stiffness of the chain, the chain's cross-sectional radius, R_c, and the contour length, L, describing the total length of the chain. To strengthen the uniqueness of the description, the parameters were matched with results from other analyses techniques: R_c was additionally derived from the Guinier relation $\ln(I(q)) \cdot q \approx R_{c,g}^2/2 \cdot q^2$ for the q-range $1.5 < qR_{c,g} < 2.1$ with $R_c = \sqrt{2}R_{c,g}$ and found to be concentration independent. The parameter b was determined by the minimum of the plot $I(q)\cdot q^2$ versus q *via* the relation $b \approx 4.6/q^*$ and subsequent extrapolation to zero concentration [27]. The contour length, L, was also determined by extrapolation, using the concentration-dependent scattering intensities $I(q)$ and $I(q)q$ with $q \to 0$ [23].

Thioflavin T assay

Thioflavin T (ThT) assays were carried out on a FLUOstar Omega (BMG Labtech GmbH, Ortenberg, Germany) reader using Greiner 96 F-bottom (non-binding) well plates

(Greiner Bio-One GmbH, Frickenhausen, Germany). All experiments were performed at 37 °C. Every 300 s, the ThT fluorescence was monitored at 480 nm with excitation at 450 nm. Samples were shaken with 300 r.p.m for 150 s prior to each excitation. The final sample volume was set to 150 µL with final concentrations of 150 µM $PTH_{1–84}$ and 50 µM ThT in citrate buffer (20 mM, pH 5.5) or sodium phosphate buffer (50 mM, pH 7.4). A series of heparin concentrations (0, 3, 7.5, 15, 30, 150, and 600 µM) was tested to assess its role in $PTH_{1–84}$ fibrillation. All measurements were done in triplicate with subsequent averaging of the ThT intensities.

Recent molecular rate kinetic descriptions of fibrillar growth enable to disentangle two main fibrillation processes [28]. While primary nucleation describes the generation of structured nuclei in the absence of fibrils, secondary pathways address the generation of nuclei on fibrillar surfaces. Both processes affect the time dependence of the fibrillar growth in a different way and hence, their contributions to the total increase in fluorescence, $\Delta F(t)$, can be analyzed using the function

$$\Delta F(t) = \left(1 - \frac{1}{\frac{\lambda^3}{3\kappa^3}\left(e^{\kappa t} - 1\right) + 1}\right)\Delta F_{\mathrm{pl}} \qquad (2)$$

where ΔF_{pl} describes the plateau of the fluorescence assay. λ and κ are the rate constants of nucleation and growth for primary and secondary processes, respectively. λ and κ comprise the individual microscopic rates of oligomerization, k_{o1} and k_{o2}, respectively, the rate of conversion of the unstructured oligomers into seeds, k_c, as well as the rate of elongation *via* monomer addition k_+ [29,30]:

$$\lambda = \left(2k_{o1}k_c k_+ m^{n1}\right)^{1/3}, \kappa = \left(2k_{o2}k_c k_+ m^{n2+1}\right)^{1/3} \qquad (3)$$

The parameter m displays the total mass of the monomers and $n1$ and $n2$ the sizes of the nuclei for each process. In this context, λ would also include heterogeneous seeding, as it might be induced by surfaces.

Transmission electron microscopy

5 µL of a 20 times dilution of the respective fibrillated sample was transferred to a 200 mesh Formvar/Carbon coated Cu grid (Plano GmbH, Wetzlar, Germany). After 3 min of waiting time, the grids were first cleaned in water for 3 × 10 s and then negatively stained with 1 percent (w/v) uranyl acetate for a further 60 s. Transmission electron microscopy (TEM) images were taken with an electron microscope (EM 900; Carl Zeiss AG, Oberkochen, Germany) at 80 kV acceleration voltage.

Determination of the critical concentration

$PTH_{1–84}$ fibrils (1 mL of 150 µM $PTH_{1–84}$ monomer) were formed in the presence of heparin (1 : 10 molar ratio) in pH 5.5 (20 mM citrate) or pH 7.4 (50 mM sodium phosphate) buffer at 37 °C and 350 r.p.m agitation for 3 h. The chosen incubation time ensured completion of fibril formation. Fibrils were pelleted *via* ultracentrifugation at 200 000 x g for 10 min. The $PTH_{1–84}$ concentration of the supernatant fraction was determined using UV spectroscopy and taken as the critical concentration, c^*.

Monomer release assay

Fibril pellets were obtained as mentioned above, resuspended in 100 µL pH 7.4 buffer (50 mM sodium phosphate, 5% mannitol), and subjected to dialysis through 20 k MWCO Slide-A-Lyzer Mini dialysis devices (Fisher Scientific GmbH, Schwerte, Germany) against 1 mL pH 7.4 buffer (50 mM sodium phosphate, 5% mannitol). The protein concentration outside of the dialysis device was determined using UV spectroscopy at several time points.

Results and discussion

Binding of $PTH_{1–84}$ to heparin

Thermodynamics of the interaction

Binding thermodynamics can provide a comprehensive view of the various types of molecular interactions that drive biomolecular association. The thermodynamic feature of the heparin-$PTH_{1–84}$ binding was accessed using isothermal titration calorimetry (ITC), which detects the heat absorbed or released along the reaction coordinate. The resulting binding isotherm, as shown in Fig. 2A, can be used to determine the enthalpy, Gibbs free energy as well as stoichiometry of binding. Using a model description of independent identical binding sites, we found the equilibrium constant of dissociation, K_D, to be (213 ± 29) nM and the stoichiometry of binding to be $n = 0.09 \pm 0.01$ corresponding to 11 $PTH_{1–84}$ molecules per heparin molecule. The negative isotherms generated by the interaction of $PTH_{1–84}$ with heparin correspond to an exothermic binding event with a Gibbs free energy change, ΔG, of (−38.0 ± 0.3) kJ·mol^{-1}. The changes in enthalpy, ΔH, and entropy, ΔS are (−-72.5 ± 1.0) kJ·mol^{-1} and (0.89 ± 0.01) kJ mol^{-1}·K^{-1}, respectively. The here determined Gibbs free energy change is in very good agreement with a previously published value of −37 kJ·mol^{-1} of Kamerzell et al. [31], who used unfractionated heparin with an average mass of 12–16 kDa compared with the larger 20 kDa heparin used in this study. While the different sizes of heparin did not seem to alter ΔG, we found the stoichiometry of binding to scale linearly with the size of the heparin molecules. While heparin molecules of the size of 20 kDa (this study) revealed a binding ratio of about 11 proteins per heparin molecule, Kamerzell et al. found in their experiments that

one 12–16 kDa heparin molecule can bind about 8 $PTH_{1–84}$ molecules. Hence, assuming an average mass of a disaccharide unit of 533 Da, one protein binds roughly 3 disaccharide units of heparin. This finding supports the beads on a string model, as previously suggested in the context of other heparin-protein systems [32,33]. Notably, a minor enthalpic deviation of about 20 $kJ \cdot mol^{-1}$ is apparent at low ligand (heparin) concentrations and could be explained by a second binding process of a higher affinity but smaller exothermic enthalpy [22]. Multi-site approaches, however, yielded a high fitting error and could not be applied.

Induction of secondary structure

Circular dichroism spectroscopy was used to compare the relative secondary structure content of $PTH_{1–84}$ in citrate buffer (20 mM, pH 5.5) in the absence and presence of heparin (see Fig. 2B). In its unbound state, $PTH_{1–84}$ gave rise to a CD spectrum with pronounced negative ellipticities close to 200 nm and a shallow minimum around 222 nm. This characteristic is typical for intrinsically disordered proteins with contributions from transient α-helices [34] and matches structural data of several PTH constructs obtained *via* X-ray crystallography and nuclear magnetic resonance spectroscopy [35–37]. In the presence of heparin, a very different CD spectrum was obtained with a loss of negative ellipticity around 200 nm and significantly stronger contribution of negative ellipticity in the range spanning 210–230 nm. Since irregular peptide structures show relatively low optical activity in the latter wavelength range, the CD spectrum suggests an increase in ordered secondary structure elements of $PTH_{1–84}$ that is governed by the interaction with heparin. The CD spectrum analysis tool BeStSel [38] revealed an enhanced α-helical content in the presence of heparin (12% without heparin, 33% with heparin) accompanied by a decrease in β-strand content (25% without heparin, 13% with heparin, see Fig. S1). Comparing pH 7.4 to pH 5.5, a similar structural content of $PTH_{1–84}$ was found, but the change in secondary structure upon heparin binding was less pronounced for pH 7.4. Based on these results it can be concluded that the polyanion heparin does not only bind $PTH_{1–84}$ at low pH, while presumably screening its positive charges, but importantly also induce a change in the ordered secondary structure content.

Size and shape of heparin-$PTH_{1–84}$ associates

Small-angle X-ray scattering experiments allow to study sizes, shapes, and mutual interactions of dissolved particles and are used to investigate the molecular arrangement of $PTH_{1–84}$ with heparin. Figure 2C displays absolute scattering intensities of solutions of $PTH_{1–84}$ and heparin (1 : 10 molar ratio), prior and after mixing. The scattering intensity profile of $PTH_{1–84}$ (black data set of Fig. 2C) agreed with the simple polymer model of a flexible chain as given by Eq. 1, yielding a radius of gyration, R_g, of (2.9 ± 0.5) nm. The applicability of this model depicts the disordered feature of the protein. In contrast to $PTH_{1–84}$, the shape of the heparin molecules (gray dataset) could be described by a semiflexible chain with a Kuhn length, b, of (19.2 ± 0.7) nm and a contour length, L, of approx. 30 nm, in agreement with literature values [23,27]. While L describes the average length of the heparin backbone, b reflects the length scale of the chain's stiffness. The radius of the chain's cross-section, R_c, is (0.45 ± 0.03) nm. Immediately after the addition of $PTH_{1–84}$, the scattering intensity of the heparin solution increased by two orders of magnitude (see the red data set of Fig. 2C). Again, according to the model of a semiflexible chain, a reasonable agreement could be achieved, without changing b or L of the aforementioned description (red line in Fig. 2C). Only the cross-section of the chain increased significantly from $R_c = (0.45 \pm 0.03)$ nm to (5.3 ± 0.2) nm, supporting the earlier mentioned beads on a string model as sketched in Fig. 2D.

With time, the scattering intensities of the described chains displayed a slightly increased scattering intensity at low q values, eventually reaching a plateau after 22 h (see colored data sets in Fig. 2C). The exponent of the arising power-law dependence, $I(q) \sim qD$, can be interpreted as the dimension, D, of a mass fractal. We found D to be 2.04, characteristic for a diffusion-limited aggregation with a preferred growth at the tips and thus reduced branching [39]. This slow and preferably linear growth of $PTH_{1–84}$-heparin constructs can be taken as a first indication for a process of fibrillar growth.

Fibrillation properties

Since $PTH_{1–84}$ needs to undergo at least a partial conformational transition from α-helices to β-strands to form cross-β-structured amyloid fibrils [14], we monitored the growth process using the structure-sensitive fluorescent dye Thioflavin T that binds to β-sheet surfaces along motifs formed by cross-β strand ladders (see Fig. 3A). In the absence of heparin, the ThT fluorescence remained at a low level throughout the measurement indicating that any potential buildup of fibrils was below the detection limit. Even after 70 h of incubation at an elevated temperature of 37 °C and

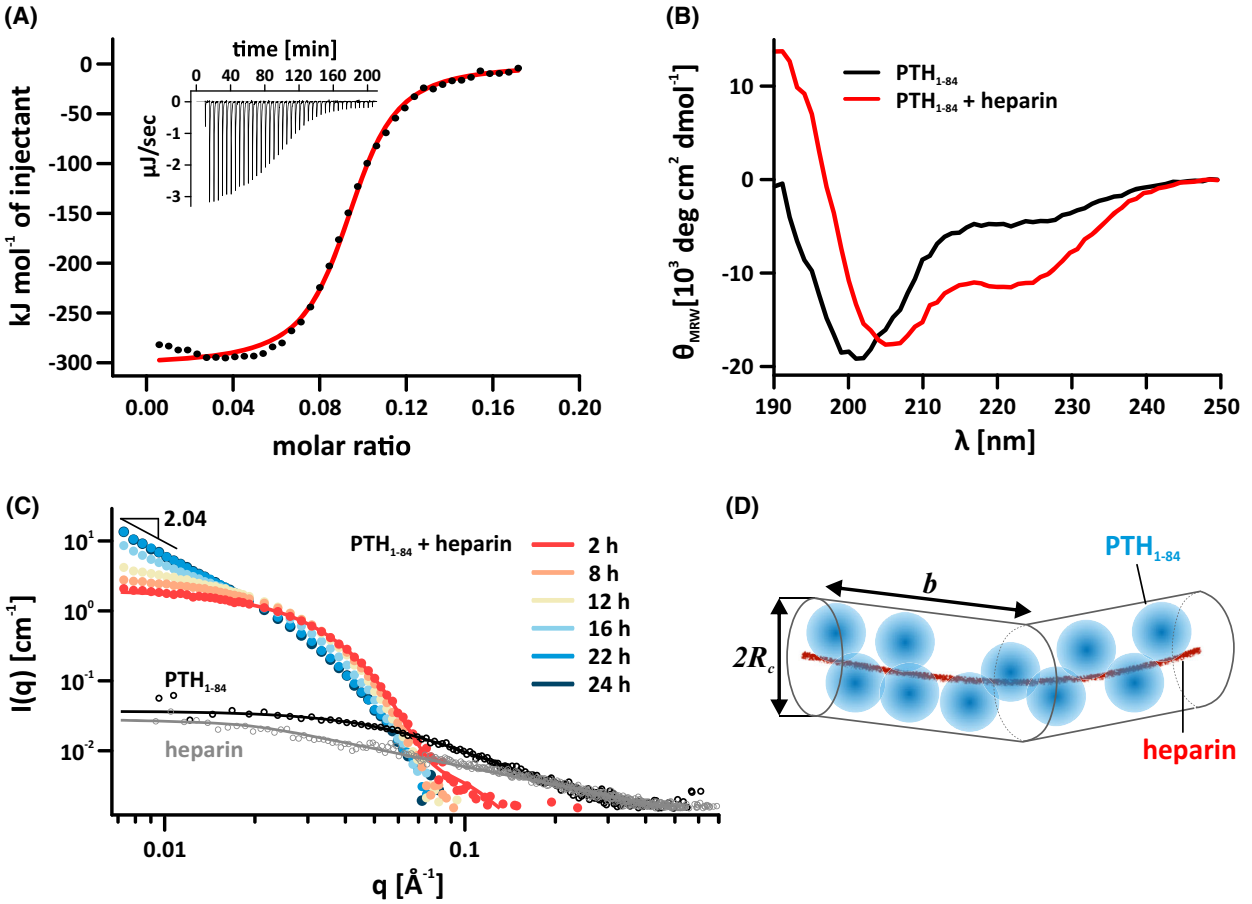

Fig. 2. Heparin binds $PTH_{1–84}$ and induces structure and aggregation. (A) Isothermal titration calorimetric data of $PTH_{1–84}$ with heparin as displayed by the integrated heat plot (dots) together with a single-site ligand-binding model fit (red line). The *x*-axis gives the molar ratio of heparin versus $PTH_{1–84}$. Inset: The raw titration data of the heat resulting from each injection of heparin into the $PTH_{1–84}$ solution. (B) CD spectrum of 100 µM $PTH_{1–84}$ in the absence (black) and presence of heparin (1 : 10 molar ratio heparin : $PTH_{1–84}$, red line). The latter was corrected for heparin contributions. (C) SAXS intensities of heparin (gray symbols), $PTH_{1–84}$ (black symbols) and a 1 : 10 molar ratio heparin : $PTH_{1–84}$ solution at different times after mixing (red to blue symbols). Lines represent adapted linear chain model functions and are described in the text. (D) Scheme of the initial $PTH_{1–84}$ binding to a single heparin molecule, as described by the model of a semiflexible linear chain (red data set in C). All measurements were performed in citrate buffer (20 mM, pH 5.5).

with orbital shaking, the fluorescence level remained virtually unchanged. Subsequent centrifugation of the sample did not yield a noticeable precipitate, suggesting that $PTH_{1–84}$ remained in its soluble, monomeric state. Conversely, $PTH_{1–84}$ rapidly formed fibrils when heparin was present with ThT plateau intensities that initially increased with heparin concentration and eventually saturated (Fig. 3C, top graph). The latter could be evidence for possible binding of heparin to the fibrillar surfaces as it was observed for fibrils of the amyloid beta peptide [40].

Notably, the initial lag phase was passing a minimum value of 0.6 h at heparin concentrations of 15 µM and 30 µM (1 : 10 and 1 : 5 ratio of heparin: $PTH_{1–84}$) indicative for a more complex interplay of aggregation processes than simple seeding. Seeding would solely lead to a concentration-dependent decrease in the lag times [41].

To infer more information regarding the dominating processes of fibrillation, we analyzed the data with respect to the total rates of primary and secondary fibrillation pathways, λ and κ, as given by Eq. 2. The fitting results are displayed in the normalized data set of Fig. 3B and the derived values of λ and κ are given in Fig. 3C, bottom graph. While λ reflects the generation of structured nuclei in the absence of fibrils, κ addresses the generation of nuclei on the surface of the growing fibrillar phase. It is important to mention that both rates comprise not only their specific microscopic rates of nucleation but also the more general rate of

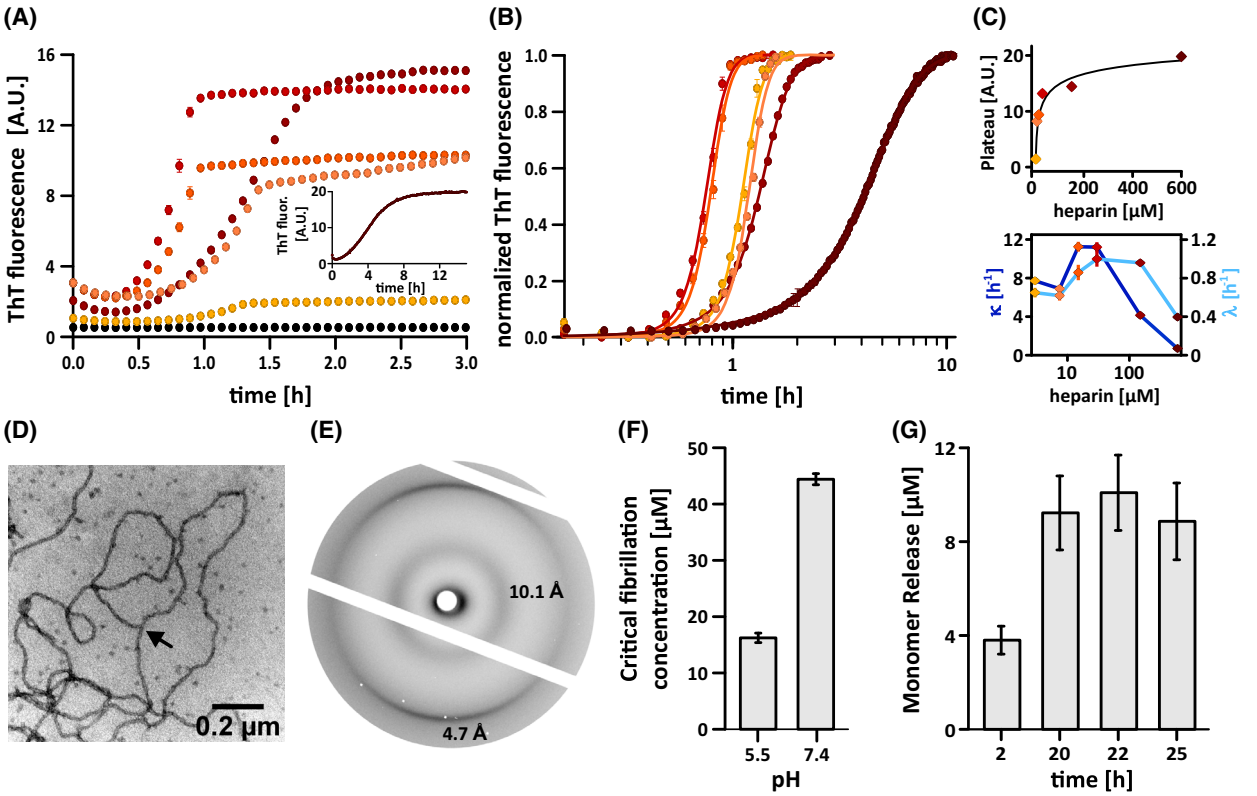

Fig. 3. Heparin induces rapid $PTH_{1–84}$ fibrillation. (A) ThT fluorescence was used to monitor fibrillation of $PTH_{1–84}$ (150 μM, 37 °C, 300 r.p.m orbital shaking) at several heparin concentrations [black—no heparin; yellow—3 μM; light orange—7.5 μM; orange—15 μM; red—30 μM; dark red—150 μM; purple (inset)—600 μM]. Solely in the presence of heparin, the ThT fluorescence increased significantly over time reaching plateau values that were depending on heparin concentration (see C top graph). Data points were averaged from triplicates and shown with standard deviation error bars. (B) Normalization of the ThT fluorescence (symbols) and subsequent fitting using Eq. 2 (lines) yielded heparin-dependent nucleation and growth rates λ (primary fibrillation pathways) and κ (secondary fibrillation pathways). (C) The plateau intensities (top graph) and λ and κ values (bottom graph) were dependent on heparin concentration. (D) Transmission electron microscope images of $PTH_{1–84}$ fibrils displayed a curvilinear structure with fibrillar branching (arrow). (E) X-ray diffraction of $PTH_{1–84}$ fibrils formed in the presence of heparin at pH 5.5. Reflections at 4.7 Å and 10.1 Å were consistent with a cross-β structure. (F) At pH 5.5, the critical concentration for fibril formation is reduced compared with pH 7.4. Fibrillation was induced with 1 : 10 molar ratio heparin:$PTH_{1–84}$. Data points were averaged from triplicates with standard deviation error bars shown. (G) $PTH_{1–84}$ fibrils formed in the presence of heparin at pH 5.5 release monomers in a time-dependent manner. Data points were averaged from triplicates with standard deviation error bars shown.

fibrillar growth *via* monomer addition (see Eq. 3). For concentrations below the critical molar ratio of 1 : 10 (heparin : $PTH_{1–84}$), one can expect that not all of the $PTH_{1–84}$ molecules are bound to heparin. For low concentrations (up to 7.5 μM, 1 : 20 ratio), we found both rates to not depend on heparin concentration. Higher heparin concentrations caused both rates to increase until a plateau of about 150% of their initial values was reached. The significant increase of κ implies that heterogeneous seeding, meaning that heparin molecules act as seeds on their own, cannot be the leading mechanism by which heparin induces fibrillation. Heterogeneous seeding would affect λ only and, hence, lead to an increase in the so-called nucleation-to-growth factor $\lambda^3/3\kappa^3$ of Eq. 2. This factor was not only small, indicative for reactions in which the nucleation step is rate-limiting [42], but also independent from the heparin concentration with, for example, $(2.0 \pm 0.2)\cdot10^{-4}$ for the 1 : 50 molar ratio and $(1.5 \pm 0.3)\cdot10^{-4}$ for the 1 : 10 molar ratio (heparin : $PTH_{1–84}$). Hence, the experimental determined increase in the overall rate could either origin from an increased rate of structural conversion into seeds, or fibrillar growth (k_c or k_+ of Eq. 3). If the latter would be true, λ and κ should be still enhanced at higher heparin concentrations, at which most of the $PTH_{1–84}$ molecules are bound to heparin. However, at heparin concentrations above the critical molar ratio of 1 : 10, we observed a plateau of λ and κ followed by a decrease (see Fig. 3C), meaning that heparin-bound $PTH_{1–84}$ can form primary and

secondary seeds but cannot contribute to the fibrillar growth as growth seems to require unbound $PTH_{1–84}$-molecules. Hence, the leading mechanism of heparin at high and low concentrations is the structural conversion of bound $PTH_{1–84}$ into amyloid-prone seeds. The morphology and structure of the mature $PTH_{1–84}$ fibrils were confirmed by electron microscopy (Fig. 3D) and X-ray diffraction (Fig. 3E). The TEM images displayed long and slightly curved fibrils of about 16 nm thickness. Branching was very rarely observed, which agrees well with the fractal dimension from the scattering experiments. WAXS experiments confirmed the cross-β sheet structure of the fibrils with characteristic reflections at 4.7 Å and 10.1 Å (Fig. 3E) [14].

The interactions of heparin/GAG with proteins are known to be dominated by electrostatics [43]. Since the charge state of $PTH_{1–84}$ is sensitive toward changes in the physiological pH range, we asked if variations in pH conditions influence fibrillation efficiency. We incubated $PTH_{1–84}$ and heparin at 37 °C for 3 h in buffers adjusted to pH 5.5 or pH 7.4 and pelleted the fibrillar content *via* ultracentrifugation (more details in material and methods). As a control, by omitting the incubation, we could confirm that heparin-$PTH_{1–84}$ complexes formed immediately after mixing could not be pelleted by ultracentrifugation, indicating that fibrils formed after 3 h are the main species pelleted. The remaining protein concentration in the supernatant should approximate the critical concentration for fibril formation assuming basic thermodynamic principles [42]. Following the described procedure, we found the critical concentrations for fibril formation, c^*, to be about 2.6-fold higher at pH 7.4 compared with pH 5.5 (Fig. 3F). This finding would imply that the conversion of monomers into fibrils is more efficient at low pH. In order to validate this finding, we additionally compared the plateau intensities of the ThT assays. Based on the crystallization model of Finke and Watzky [42], plateau values of ThT assays, ΔF_{pl}, are not only directly correlated to the fibrillar mass but also to the supersaturation of the solution, $\sigma = (c - c^*)/c^*$ [42]. These considerations lead to the equation:

$$c^*_{pH7.4}/c^*_{pH5.5} \approx c/c^*_{pH5.5} - \left(\Delta F_{pl}^{pH7.4}/\Delta F_{pl}^{pH5.5}\right)\left(c/c^*_{pH5.5} - 1\right),$$

where c is the total protein concentration of the experiment. Using the experimentally derived value $c^*_{pH5.5}$ of 17 {M and the independently obtained ThT plateau intensities of the $PTH_{1–84}$ fibrillation (see Fig. S2), these considerations would lead to a ratio $c^*_{pH7.5}/c^*_{pH5.5}$ of 3.2. This value is slightly larger than from the above-mentioned ultracentrifugation experiments, but in the same range. The difference could originate, for example, from surface charges that are present at low pH and modify the interaction of ThT with fibrils [44]. Possible pH-dependent spectral changes in ThT were considered by control measurements. Surprisingly, the obtained ratio of the critical concentrations would be equivalent to just a small additional gain in free energy of $\Delta(\Delta G) \approx 2.6 – 2.8$ kJ·mol^{-1} according to the relation $\Delta(\Delta G) = -\mathrm{RTln}\left(c^*_{7.4}/c^*_{5.5}\right)$. Hence, lowering the pH leads to a small, but significant change in ΔG compared with the total gain of free energy for amyloid fibrillation that is about 30–50 kJ·mol^{-1} [45].

The described pH dependence points to a mainly charge-driven interaction of heparin with $PTH_{1–84}$ that is modulated by the protonation state of the four histidine residues within the peptide chain. Due to their unique pK_A value close to the physiological pH (pH ≈ 6.2), histidine side chains are mainly protonated at pH 5.5 while unprotonated at pH 7.4. Therefore, histidines display a pH-dependent switch-like property that is key in many biochemical processes including pH sensoric function [46,47]. This switch-like property has previously been identified to modulate protein–GAG interactions [48].

However, even accounting for protonated histidines, $PTH_{1–84}$ lacks a classical heparin-binding consensus sequence (XBBXBX and XBBBXXBX, where B is a basic residue and X is a hydropathic residue) [49]. Importantly though, heparin-binding proteins lacking these particular amino acid sequences are well known [50]. They may instead bind heparin through a structurally similar binding motif, in which the involved residues are spatially close but may be distant in the primary sequence [50]. This binding modality seems particularly intriguing in the case of the largely disordered $PTH_{1–84}$, which might dynamically adopt a high-affinity heparin-binding state with particular amino acids arranged in a structural heparin-binding motif. At low pH, this structural binding motif might be partially formed by protonated histidines within $PTH_{1–84}$, while being interrupted when histidines are unprotonated at neutral pH. Similarly, it has already been reported that seemingly minute differences in the sequence of peptides can have significant effects on the GAG-mediated fibril formation [51].

To get a more detailed view on the binding sites of $PTH_{1–84}$ for GAGs, we recorded a residue resolved 2D NMR experiment in the presence and absence of fondaparinux (Fig. S3). Fondaparinux is a pentameric heparin sulfate analog with a well-defined molecular weight of 1728 Da and suitable in size for NMR spectroscopy [52]. We observed binding within the first 40 residues, which contain H10, K13, H14, R20, R25,

K26, K27, and H32 with the latter four residues contributing to the fibrillar core [14]. Additionally, the positive stretch R52, K53, and K54 reported binding. Along this line, our data indicate that $PTH_{1–84}$ fibrillation in the presence of heparin does not only overcome fibrillation retarding side chain protonation due to charge repulsion, but results even in a remarkably higher fibrillation efficiency compared with neutral pH.

Monomer release of $PTH_{1–84}$ fibrils

Functional amyloid fibrils typically are reversible structures capable of releasing monomers in solution [53–56]. Various structures of PTH and related peptides in complex with their target receptor PTH1R show a protrusion of the ligand deep into a tight cavity of the receptor [57–59]. Hence, it is likely that monomeric $PTH_{1–84}$ is required for receptor stimulation. We tested whether $PTH_{1–84}$ fibrils formed at pH 5.5 in the presence of heparin-released monomers in a neutral pH buffer. We used a dialysis approach with a cutoff filter of 20 k MWCO to let $PTH_{1–84}$ monomers pass the membrane and dialyzed against buffer adjusted to pH 7.4 to resemble the blood pH (see Method section). Under these conditions, we found the $PTH_{1–84}$ monomer concentration outside of the dialysis membrane increasing over time (Fig. 3F), suggesting a time-dependent monomer release. This is in accordance with similar functional amyloid [53,60] and confirms an earlier report by Gopalswamy et al., [14] who found $PTH_{1–84}$ fibrils to release monomers in a similar manner.

In summary, a major goal of our *in vitro* experiments was to mimic two key environmental properties that may affect the fibrillation of $PTH_{1–84}$ in the cellular context (Fig. 1A): We adjusted the pH to a moderately acidic value (pH 5.5) to approximate the conditions in which $PTH_{1–84}$ fibrils are supposed to form *in vivo*. We combined the low pH conditions with the addition of heparin, as the Golgi apparatus is the major site for the synthesis of GAGs. The use of the GAG heparin allowed us to study the effect of a polyanionic linear macromolecule that is in close resemblance of what $PTH_{1–84}$ might interact with during intracellular transport.

Under the conditions tested, we found that the largely intrinsically disordered $PTH_{1–84}$ binds with a submicromolar affinity to heparin and heparin is indispensable for rapid $PTH_{1–84}$ fibril formation. Strikingly, binding to heparin changed not only the ordered secondary structure content and induced fibrillation, but enabled even more efficient fibrillation at low pH compared with neutral pH. Notably, the mean β-strand content as determined by CD spectroscopy did not correlate with individual seeding capabilities (comparison of $PTH_{1–84}$ free and bound to heparin at low pH) nor fibrillation efficiencies (comparison of $PTH_{1–84}$ fibrillation with heparin at high and low pH) for heparin-$PTH_{1–84}$ associates. This finding underscores the importance of heparin or equivalent polyanionic structures and their interactions during protein assembly.

The enhanced kinetic of fibrillation in the presence of heparin is consistent with the potentially short lifetime of the peptide hormone in the cells as indicated by previously conducted pulse-chase experiments that show a cellular secretion of $PTH_{1–84}$ as soon as 30 min after its translation [61,62]. This is in line with the general properties of functional amyloids, which need to form more rapidly compared with disease-associated fibrils [63]. Mechanistically, heparin forms a semiflexible chain assembly decorated with several $PTH_{1–84}$ molecules, which induces fibril formation by enhancing primary and secondary nucleation pathways likewise. The heparin-assisted fibrillar growth at low pH further suggests that $PTH_{1–84}$ fibril formation might follow a similar mechanism in the cellular context possibly relying on endogenous GAGs or glycosylated proteins. This is further supported by earlier studies which revealed that $PTH_{1–84}$ is co-stored and co-secreted with proteoglycans [62,64]. The high efficiency of fibril formation as indicated by a reduced critical fibrillation concentration at the lower pH suggests that the polyanion-driven $PTH_{1–84}$ fibrillation is enhanced under pH conditions present in later stages of the secretory pathway, for example, the trans-Golgi network and secretory granules. The pH sensitivity of this process might have a regulating function for sorting and further transport of $PTH_{1–84}$. A regulatory role of the GAG-assisted formation of functional amyloid fibrils in the secretory pathway was previously proposed [7].

Acknowledgements

The authors acknowledge funding by the German Science Foundation (DFG) under Project No. 391498659 (RTG 2467) and Project No. 189853844 (CRC TRR 102). The authors thank for the kind experimental support of Stephan M. Feller of the Institute of Molecular Medicine of the Martin-Luther University Halle-Wittenberg (ITC) and of Thomas Thurn-Albrecht of the Institute of Physics of the Martin-Luther University Halle-Wittenberg (SAXS).

Author contributions

MO and LL designed the research and wrote the manuscript. LL performed the majority of the experimental work and data analysis, NMR and TEM experiments were performed and analyzed by BV, SAXS experiments were conducted by TB, LM provided the expertise for ITC experiments. MO and JB supervised experiments, data analysis and discussion. All authors reviewed the results and approved the final version of the manuscript.

Data accessibility

Data are available on request from the authors.

References

1 Habener JF, Rosenblatt M, Potts JJT. Parathyroid hormone: biochemical aspects of biosynthesis, secretion, action, and metabolism. *Physiol Rev*. 1984;**64**:985–1053.
2 Usdin TB. The PTH2 receptor and TIP39: a new peptide–receptor system. *Trends Pharmacol Sci*. 2000;**21**:128–30.
3 Jüppner H, Abou-Samra A-B, Freeman M, Kong XF, Schipani E, Richards J, et al. A G protein-linked receptor for parathyroid hormone and parathyroid hormone-related peptide. *Science*. 1991;**254**:1024–6.
4 Gensure RC, Gardella TJ, Jüppner H. Parathyroid hormone and parathyroid hormone-related peptide, and their receptors. *Biochem Biophys Res Commun*. 2005;**328**:666–78.
5 Michael DJ, Cai H, Xiong W, Ouyang J, Chow RH. Mechanisms of peptide hormone secretion. *Trends Endocrinol Metab*. 2006;**17**:408–15.
6 Paroutis P, Touret N, Grinstein S. The pH of the secretory pathway: measurement, determinants, and regulation. *Physiology*. 2004;**19**:207–15.
7 Maji SK, Perrin MH, Sawaya MR, Jessberger S, Vadodaria K, Rissman RA, et al. Functional amyloids as natural storage of peptide hormones in pituitary secretory granules. *Science*. 2009;**325**:328–32.
8 Dannies PS. Prolactin and growth hormone aggregates in secretory granules: the need to understand the structure of the aggregate. *Endocr Rev*. 2012;**33**:254–70.
9 Anderson TJ, Ewen SWB. Amyloid in normal and pathological parathyroid glands. *J Clin Pathol*. 1974;**27**:656–63.
10 Furukawa K, Aguirre C, So M, Sasahara K, Miyanoiri Y, Sakurai K, et al. Isoelectric point-amyloid formation of α-synuclein extends the generality of the solubility and supersaturation-limited mechanism. *Curr Res Struct Biol*. 2020;**2**:35–44.
11 Nespovitaya N, Gath J, Barylyuk K, Seuring C, Meier BH, Riek R. Dynamic assembly and disassembly of functional β-endorphin amyloid fibrils. *J Am Chem Soc*. 2016;**138**:846–56.
12 Marek PJ, Patsalo V, Green DF, Raleigh DP. Ionic strength effects on amyloid formation by amylin are a complicated interplay among Debye screening, ion selectivity, and Hofmeister effects. *Biochemistry*. 2012;**51**:8478–90.
13 Calculated using the Protein Tool protpi. [cited 2021 May 8]. Available from: https://www.protpi.ch/Calculator/ProteinTool
14 Gopalswamy M, Kumar A, Adler J, Baumann M, Henze M, Kumar ST, et al. Structural characterization of amyloid fibrils from the human parathyroid hormone. *Biochim Biophys Acta*. 2015;**1854**:249–57.
15 Priyadarshini M, Bano B. Conformational changes during amyloid fibril formation of pancreatic thiol proteinase inhibitor: effect of copper and zinc. *Mol Biol Rep*. 2012;**39**:2945–55.
16 Lima M, Rudd T, Yates E. New applications of heparin and other glycosaminoglycans. *Molecules*. 2017;**22**:749.
17 Dick G, Akslen-Hoel LK, Grøndahl F, Kjos I, Prydz K. Proteoglycan synthesis and golgi organization in polarized epithelial cells. *J Histochem Cytochem*. 2012;**60**:926–35.
18 Prydz K. Determinants of glycosaminoglycan (GAG) structure. *Biomolecules*. 2015;**5**:2003–22.
19 Wall JS, Richey T, Stuckey A, Donnell R, Macy S, Martin EB, et al. In vivo molecular imaging of peripheral amyloidosis using heparin-binding peptides. *Proc Natl Acad Sci U S A*. 2011;**108**:E586–94.
20 Kumar A, Gopalswamy M, Wishart C, Henze M, Eschen-Lippold L, Donnelly D, et al. N-terminal phosphorylation of parathyroid hormone (PTH) abolishes its receptor activity. *ACS Chem Biol*. 2014;**9**:2465–70.
21 Keller S, Vargas C, Zhao H, Piszczek G, Brautigam CA, Schuck P. High-precision isothermal titration calorimetry with automated peak-shape analysis. *Anal Chem*. 2012;**84**:5066–73.
22 Le VH, Buscaglia R, Chaires JB, Lewis EA. Modeling complex equilibria in isothermal titration calorimetry experiments: thermodynamic parameters estimation for a three-binding-site model. *Anal Biochem*. 2013;**434**:233–41.
23 Pavlov G, Finet S, Tatarenko K, Korneeva E, Ebel C. Conformation of heparin studied with macromolecular hydrodynamic methods and X-ray scattering. *Eur Biophys J*. 2003;**32**:437–49.
24 Roe RJ. Methods of X-ray and neutron scattering in polymer science. New York: Oxford University Press; 2000.
25 Pedersen JS, Schurtenberger P. Scattering functions of semiflexible polymers with and without excluded volume effects. *Macromolecules*. 1996;**29**:7602–12.

26 Chen W-R, Butler PD, Magid LJ. Incorporating Intermicellar interactions in the fitting of SANS data from cationic wormlike micelles. *Langmuir*. 2006;**22**:6539–48.

27 Khorramian B, Stivala S. Small-angle x-ray scattering of high- and low-affinity heparin. *Arch Biochem Biophys*. 1986;**247**:384–92.

28 Meisl G, Rajah L, Cohen SAI, Pfammatter M, Šarić A, Hellstrand E, et al. Scaling behaviour and rate-determining steps in filamentous self-assembly. *Chem Sci*. 2017;**8**:7087–97.

29 Michaels TCT, Šarić A, Curk S, Bernfur K, Arosio P, Meisl G, et al. Dynamics of oligomer populations formed during the aggregation of Alzheimer's Aβ42 peptide. *Nat Chem*. 2020;**12**:445–51.

30 Dear AJ, Michaels TCT, Meisl G, Klenerman D, Wu S, Perrett S, et al. Kinetic diversity of amyloid oligomers. *Proc Natl Acad Sci U S A*. 2020;**117**:12087–94.

31 Kamerzell TJ, Joshi SB, Mcclean D, Peplinskie L, Toney K, Papac D, et al. Parathyroid hormone is a heparin/polyanion binding protein: binding energetics and structure modification. *Protein Sci*. 2007;**16**:1193–203.

32 Venkataraman G, Sasisekharan V, Herr AB, Ornitz DM, Waksman G, Cooney CL, et al. Preferential self-association of basic fibroblast growth factor is stabilized by heparin during receptor dimerization and activation. *Proc Natl Acad Sci U S A*. 1996;**93**:845–50.

33 Kuschert GSV, Coulin F, Power CA, Proudfoot AEI, Hubbard RE, Hoogewerf AJ, et al. Glycosaminoglycans interact selectively with chemokines and modulate receptor binding and cellular responses. *Biochemistry*. 1999;**38**:12959–68.

34 Kelly SM, Jess TJ, Price NC. How to study proteins by circular dichroism. *Biochim Biophys Acta*. 2005;**1751**:119–39.

35 Chen Z, Xu P, Barbier J-R, Willick G, Ni F. Solution structure of the osteogenic 1–31 fragment of the human parathyroid hormone. *Biochemistry*. 2000;**39**:12766–77.

36 Marx UC, Adermann K, Bayer P, Forssmann W-G, Rösch P. Solution structures of human parathyroid hormone fragments hPTH(1–34) and hPTH(1–39) and bovine parathyroid hormone fragment bPTH(1–37). *Biochem Biophys Res Commun*. 2000;**267**:213–20.

37 Jin L, Briggs SL, Chandrasekhar S, Chirgadze NY, Clawson DK, Schevitz RW, et al. Crystal structure of human parathyroid hormone 1–34 at 0.9-Å resolution. *J Biol Chem*. 2000;**275**:27238–44.

38 Micsonai A, Bulyàki E, Kardos J. BeStSel: from secondary structure analysis to protein fold prediction by circular dichroism spectroscopy. *Methods Mol Biol*. 2021;**2199**:175–89.

39 Nicolás-Carlock JR, Carrillo-Estrada JL. A universal dimensionality function for the fractal dimensions of Laplacian growth. *Sci Rep*. 2019;**9**:1120.

40 Madine J, Pandya MJ, Hicks MR, Rodger A, Yates EA, Radford SE, et al. Site-specific identification of an Aβ fibril-heparin interaction site by using solid-state NMR spectroscopy. *Angew Chem Int Ed*. 2012;**51**:13140–3.

41 Cukalevski R, Yang X, Meisl G, Weininger U, Bernfur K, Frohm B, et al. The Aβ40 and Aβ42 peptides self-assemble into separate homomolecular fibrils in binary mixtures but cross-react during primary nucleation. *Chem Sci*. 2015;**6**:4215–33.

42 Crespo R, Rocha FA, Damas AM, Martins PM. A generic crystallization-like model that describes the kinetics of amyloid fibril formation. *J Biol Chem*. 2012;**287**:30585–94.

43 Lander AD. Targeting the glycosaminoglycan-binding sites on proteins. *Chem Biol*. 1994;**1**:73–8.

44 Arad E, Green H, Jelinek R, Rapaport H. Revisiting thioflavin T (ThT) fluorescence as a marker of protein fibrillation – the prominent role of electrostatic interactions. *J Colloid Interface Sci*. 2020;**573**:87–95.

45 Baldwin AJ, Knowles TPJ, Tartaglia GG, Fitzpatrick AW, Devlin GL, Shammas SL, et al. Metastability of native proteins and the phenomenon of amyloid formation. *J Am Chem Soc*. 2011;**133**:14160–3.

46 Mideros-Mora C, Miguel-Romero L, Felipe-Ruiz A, Casino P, Marina A. Revisiting the pH-gated conformational switch on the activities of HisKA-family histidine kinases. *Nat Commun*. 2020;**11**:769.

47 Wu W, Celma CC, Kerviel A, Roy P. Mapping the pH sensors critical for host cell entry by a complex nonenveloped virus. *J Virol*. 2019;**93**:e01897–18.

48 Elimova E, Kisilevsky R, Ancsin JB. Heparan sulfate promotes the aggregation of HDL-associated serum amyloid a: evidence for a proamyloidogenic histidine molecular switch. *FASEB J*. 2009;**23**:3436–48.

49 Cardin AD, Weintraub HJ. Molecular modeling of protein-glycosaminoglycan interactions. *Arteriosclerosis*. 1989;**9**:21–32.

50 Muñoz EM, Linhardt RJ. Heparin-binding domains in vascular biology. *Arterioscler Thromb Vasc Biol*. 2004;**24**:1549–57.

51 Jha NN, Anoop A, Ranganathan S, Mohite GM, Padinhateeri R, Maji SK. Characterization of amyloid formation by glucagon-like peptides: role of basic residues in heparin-mediated aggregation. *Biochemistry*. 2013;**52**:8800–10.

52 Gao Q, Yang J-Y, Moremen KW, Flanagan JG, Prestegard JH. Structural characterization of a heparan sulfate pentamer interacting with LAR-Ig1-2. *Biochemistry*. 2018;**57**:2189–99.

53 Jackson MP, Hewitt EW. Why are functional amyloids non-toxic in humans? *Biomolecules*. 2017;**7**:71.

54 Jacob RS, Das S, Ghosh S, Anoop A, Jha NN, Khan T, et al. Amyloid formation of growth hormone in presence of zinc: relevance to its storage in secretory granules. *Sci Rep*. 2016;**6**:23370.

55 Anoop A, Ranganathan S, Dhaked BD, Jha NN, Pratihar S, Ghosh S, et al. Elucidating the role of disulfide bond on amyloid formation and fibril reversibility of Somatostatin-14. *J Biol Chem*. 2014;**289**:16884–903.
56 Maji SK, Schubert D, Rivier C, Lee S, Rivier JE, Riek R. Amyloid as a depot for the formulation of long-acting drugs. *PLoS Biol*. 2008;**6**:e17.
57 Zhao L-H, Ma S, Sutkeviciute I, Shen DD, Zhou XE, de Waal PW, et al. Structure and dynamics of the active human parathyroid hormone receptor-1. *Science*. 2019;**364**:148–53.
58 Pioszak AA, Xu HE. Molecular recognition of parathyroid hormone by its G protein-coupled receptor. *Proc Natl Acad Sci U S A*. 2008;**105**:5034–9.
59 Pioszak AA, Parker NR, Gardella TJ, Xu HE. Structural basis for parathyroid hormone-related protein binding to the parathyroid hormone receptor and Design of Conformation-selective Peptides. *J Biol Chem*. 2009;**284**:28382–91.
60 Chatterjee D, Jacob RS, Ray S, Navalkar A, Singh N, Sengupta S, et al. Co-aggregation and secondary nucleation in the life cycle of human prolactin/galanin functional amyloids. *Elife*. 2022;**11**:e73835.
61 Habener JF, Amherdt M, Ravazzola M, Orci L. Parathyroid hormone biosynthesis. Correlation of conversion of biosynthetic precursors with intracellular protein migration as determined by electron microscope autoradiography. *J Cell Biol*. 1979;**80**:715–31.
62 Muresan Z, Macgregor RR. The release of parathyroid hormone and the exocytosis of a proteoglycan are modulated by extracellular Ca2+ in a similar manner. *Mol Biol Cell*. 1994;**5**:725–37.
63 Otzen D, Riek R. Functional amyloids. *Cold Spring Harb Perspect Biol*. 2019;**11**:a033860.
64 Gorr SU, Hamilton JW, Cohn DV. Sulfated secreted forms of bovine and porcine parathyroid chromogranin a (secretory protein-I). *J Biol Chem*. 1991;**266**:5780–4.

Supporting information

Additional supporting information may be found online in the Supporting Information section at the end of the article.

Fig. S1. Buffer effect on circular dichroism spectra of PTH_{1-84} in absence and presence of heparin (1 : 10 molar ratio heparin : PTH_{1-84}).

Fig. S2. Buffer effect on ThT curves of PTH_{1-84} in presence of heparin (1 : 10 molar ratio heparin : PTH_{1-84}).

Fig. S3. NMR detected interaction of PTH_{1-84} with fondaparinux.